Dynamic analysis of voltage angle droop controlled HVDC systems in curative congestion management scenarios

Yang Zhou[1,*], *Stefan* Dalhues[1], and *Ulf* Häger[1]

[1]Institute of Energy Systems, Energy Efficiency and Energy Economics (ie[3]), TU Dortmund University, 44227 Dortmund, Germany

Abstract. The integration of the voltage-source converter based high voltage direct current (VSC-HVDC) system makes the set-point of its active power adaptive to the changes in the power flow, and contributes to the curative congestion management. To further exploit the dynamic behavior of a hybrid AC/DC power system in curative congestion management scenarios, this paper investigates a novel control scheme for voltage angle droop controlled HVDC (VAD-HVDC) systems. The proposed scheme to alleviate the circuit overload is estimated firstly by calculating the severity index when the power flow changes under N-1 situations. Then the voltage angle controlled HVDC system is applied on the modified IEEE 39-bus 10-machine test power system for the time-domain simulation. The dynamic behavior in the HVDC station validates that the VAD control can stabilize the DC voltage and possess a good ability against interference. In addition, the dynamic characteristics analysis on the AC transmission lines proves that the hybrid AC/DC system integrated with the VAD controlled HVDC system are in possession of good stability after the N-1 contingency event. The VAD controller employed in the HVDC system is capable of effective congestion management to mitigate the critical loadings on the transmission lines.

Introduction

Considering the energy transition in Germany, many wind turbines are installed in northern Germany and traditional power plants are shut down in the south. The current AC transmission lines are not enough to transmit massive power from the north to the south. Therefore, several HVDC corridors are under construction in Germany to transmit power over long distances from the main power generation center to the main load center [1]. These HVDC corridors will be embedded in the AC grid to offer a number of technical and economic advantages for the transmitting and sharing of reserves.

At the same time, the operational planning of electrical networks is based upon the N-1 criterion for ensuring operational safety in general. As a result, a large part of the existing network capacity is not used to compensate for the failure of a resource in the network. In order to increase the transmission capacity of the network, curative network congestion management can be undertaken [2, 3]. In doing so, it is permitted that certain N-1 cases in the network can first trigger overload situations, which are then alleviated or resolved by means of corrective measures [4]. To this end, HVDC corridors can be used as power flow regulating equipment to counteract this in case of an N-1 scenario.

In recent years, the research of HVDC systems for network congestion management in hybrid AC/DC power systems has attracted wide attention. A mixed AC/DC OPF as one possibility to generate a schedule for HVDC converters to react to changes of power flow is presented in [5, 6]. An automated method, which minimizes transmission losses while including the AC line loadings as limits for the HVDC power is proposed in [7, 8]. An optimal placement and control variable setting of power flow controllers in multi-terminal HVDC grids is shown in [9] for enhancing static security. The approach presented in [10] concerns static aspects and slow stability phenomena introduced by AC-related contingencies. Therefore, the majority of literature regarding utilization of HVDC system for congestion management is traditionally performed on the basis of static analysis.

However, in addition to static performance index, system security also comprises dynamic stability and transient response [11]. A dynamic control strategy implemented by adding a control signal to the DC current reference of the rectifier current regulator is proposed in [12] for HVDC links to relieve transmission lines overloads during emergencies. A novel remedial action scheme is evaluated in [13] by both static analysis and dynamic response to solve the congestion problem. Up to now, there is rare research concerning the dynamic process of a hybrid AC/DC system in congestion management scenarios. More consideration should be given to dynamic analysis and time-domain simulations involved in the issue of the usage of HVDC links for alleviating congestion in power systems.

Based upon the aforementioned problem, this paper focuses on achieving good dynamic performance and control capability by further exploiting the dynamic behavior of the proposed voltage angle droop (VAD)

* Corresponding author: yang.zhou@tu-dortmund.de

© The Authors, published by EDP Sciences. This is an open access article distributed under the terms of the Creative Commons Attribution License 4.0 (http://creativecommons.org/licenses/by/4.0/).

control. The VAD method used in this paper was first proposed and designed in detail in [14]. It has been verified in our recent work that this method is very efficient to alleviate the overloads for a change in power flow due to an N-1 contingency or a change in load demand. In this paper, theoretical analysis is initiated to derive the control mechanism. Then, severity index is used to indicate the curative congestion management capability. Moreover, dynamic responses are performed and analyzed to validate the control performance of the VAD controlled HVDC system in the hybrid AC/DC system.

The remainder of the paper is organized as follows. Section 2 presents the global control structure of the VSC-HVDC system and analytically derives the theory of the proposed VAD control. Section 3 describes the power flow calculation of the hybrid AC/DC system with the integration of the HVDC system. Besides, it introduces a severity index to assess the global overload situation. Section 4 firstly shows the results of the performance index under the proposed control using the modified IEEE 39-bus 10-machine system. Then the dynamic simulation results of applying the proposed method in the hybrid AC/DC dynamic model are demonstrated. Finally, the conclusion and future directions of research are given in Section 5.

2 Control of the VAD-HVDC system

A simplified diagram for the VSC-HVDC system consists of DC cables and two VSC stations connected respectively to the point 1 of common coupling (PCC1) and PCC2 via a reactor and a transformer described in Fig. 1. A set of VSC converters is embedded in the VSC converter station block in the diagram, which is employed for the AC/DC or DC/AC power conversion.

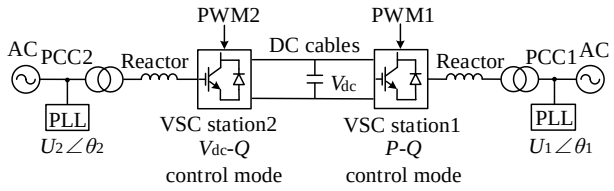

Fig. 1. A simplified diagram for the VSC-HVDC system.

The proposed control structure specially aimed at the VAD controlled HVDC system is illustrated in detail in Fig. 2. Four critical blocks including the dq current control block, real and reactive power control block, and voltage angle droop control are involved in the proposed control system in Fig. 2. The control system is realized by a fast and decoupled dq current control [15]. The current controller produces the PWM signal for the VSC station. The real and reactive power controller provide references of the dq current control. The set-point of the active power control can be obtained by the VAD control. The principle of the VAD control is elaborated and derived in the following paragraphs.

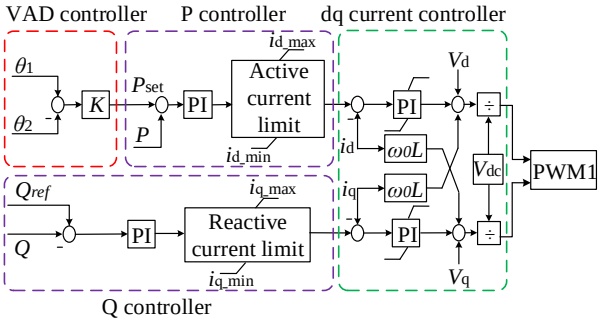

Fig. 2. Control diagram of the voltage angle droop controlled HVDC system.

The approximate linear model is well appreciated because it is faster and more convenient for the modelling and computation, compared with other models. It is assumed that the node voltages V_i, V_j are 1.0 p.u. at all nodes. When conducting the DC power flow model, the node voltage or reactive power flows can be tracked. The DC load flow suggests that there is a linear relation between the active power injections and the phase angles of nodal voltages, which can be further described as follows [16, 17].

$$P_{ij} = \frac{V_i V_j}{x_{ij}} \sin\theta_{ij} \approx \frac{1}{x_{ij}}(\theta_i - \theta_j) \tag{1}$$

where P_{ij} and x_{ij} are the branch active power flows and branch reactance; respectively at bus i and j, θ_i, θ_j are the corresponding voltage angles.

The VAD control method is further modified and improved according to (1). The reciprocal of the resistance in (1) is replaced by a gain parameter K. Consequently, the power flowing value on the HVDC line can be expressed by the DC power flow as:

$$P_{\text{set}} = K \cdot (\theta_1 - \theta_2) \tag{2}$$

where K is a droop gain; θ_1 and θ_2 denote the voltage angles collected by phase-locked loop (PLL) at PCC1 and PCC2 in Fig. 1. P_{set} denotes the DC power setting per-unit value.

The analysis above reveals that the voltage angle difference decides the power flow on the HVDC system. When the gain K is exactly equal to the inverse of line resistance, similar performances as a normal AC line will appear in the HVDC system in terms of the active power transmission. Also additional flexibility can be achieved by regulating the droop gain K accordingly. Therefore, a fast response can be made to the power flow change by the operator. The VAD control has the advantage of simplicity, because of the linear relationship between the HVDC power and the voltage angle difference. Only the terminal voltage angles of the HVDC system are essential for the control algorithm (communication time during data acquisition is not considered in this paper).

3 Calculation of AC/DC power flow

After the HVDC line is introduced into the AC power grid, power flow calculation of the hybrid AC/DC network should be considered in this section to obtain the active power of every line in the grid. Then, based

upon the calculation of power flow, severity index is defined to assess the network congestion severity, with provided generation, loading and control conditions.

The sensitivities of the branch flows with respect to the nodal real power injection changes can be computed by the DC power flow model [18]. Then a matrix $\Delta \boldsymbol{P}_l$ represents the changes in power flow on the AC lines can be calculated as:

$$\Delta \boldsymbol{P}_l = \boldsymbol{H} \cdot \Delta \boldsymbol{P}_b \tag{3}$$

where $\boldsymbol{H}$ denotes a sensitivity matrix, then the element h_{mn} is the sensitivity which means the change in the real power flow in branch m given a unit increase in the power injected at bus n; $\Delta \boldsymbol{P}_b$ is the change in nodal real power injection.

The direction matrix of HVDC injected power need to be taken into account in the AC/DC power system. Except for the connection points of HVDC, the other row's values of $\boldsymbol{D}$ are zero, which represents that the node is not connected with HVDC. Consequently, it can be described as:

$$\boldsymbol{D} = \begin{bmatrix} 0 & \cdots & 1 & -1 & \cdots & 0 \end{bmatrix}^T \tag{4}$$

where $\boldsymbol{D}$ is a $n \times 1$ column vector; n is the number of buses; 1 and -1 mean the direction of the sending and receiving terminals of the HVDC link.

Then, the $\Delta \boldsymbol{P}_b$ in the hybrid AC/DC system can be derived:

$$\Delta \boldsymbol{P}_b = \boldsymbol{D} \cdot P_{\text{set}} = \boldsymbol{D} \cdot K \cdot (\theta_1 - \theta_2) \tag{5}$$

The resulting active power $\boldsymbol{P}$ of AC lines in the AC/DC power system can be expressed as follows based upon (3) and (5):

$$\boldsymbol{P} = \boldsymbol{P}_l + \Delta \boldsymbol{P}_l = \boldsymbol{P}_l + \boldsymbol{H} \cdot \boldsymbol{D} \cdot K \cdot (\theta_1 - \theta_2) \tag{6}$$

where $\boldsymbol{P}$ is a $m \times 1$ column vector which contains the resulting power flow of all AC lines in the hybrid AC/DC system; $\boldsymbol{P}_l$ is a $m \times 1$ column vector, where the element in row m means the power flow of ac branch m in normal AC systems without HVDC links.

Network congestion during the process of power transmission can easily cause security problems. After the aforementioned calculation of the AC/DC power flow. The severity index (SI) is introduced to indicate the network congestion severity in the power system [19]:

$$SI = \sum_{i=1}^{m} \frac{p_i}{p_i^{\max}} = \sum_{i=1}^{m} \frac{p_{li} + \boldsymbol{h}_i \cdot \boldsymbol{D} \cdot P_{\text{set}}}{p_i^{\max}} \tag{7}$$

where p_i is the element in row i of vector $\boldsymbol{P}$, and denotes the resulting active power in the hybrid AC/DC power system; $p_i^{\max}$ represents the upper active power limit in branch i; p_{li} is the element in row i of vector the change in power flow on the AC line i; h_i is the row vector in row i of matrix $\boldsymbol{H}$.

4 Simulation and results

The performance of the proposed VAD controlled HVDC system is assessed and analyzed based upon a hybrid AC/DC system in this section. At first, the severity index is calculated. Then, the dynamic behavior of the hybrid AC/DC integrated with the HVDC system is observed and exploited to verify the dynamic performance.

4.1 Topology of the hybrid AC/DC simulation system

Test cases are carried out on a hybrid AC/DC test system, which is a modified New England Test System. A single-line diagram of the hybrid AC/DC test system is illustrated in Fig. 3. The test system comprises 39 buses, 10 synchronous generators and 46 transmission lines. Then an HVDC system is built between bus 15 and 4. The dynamic system is established and simulated in DIgSILENT PowerFactory 2019 [20] [21].

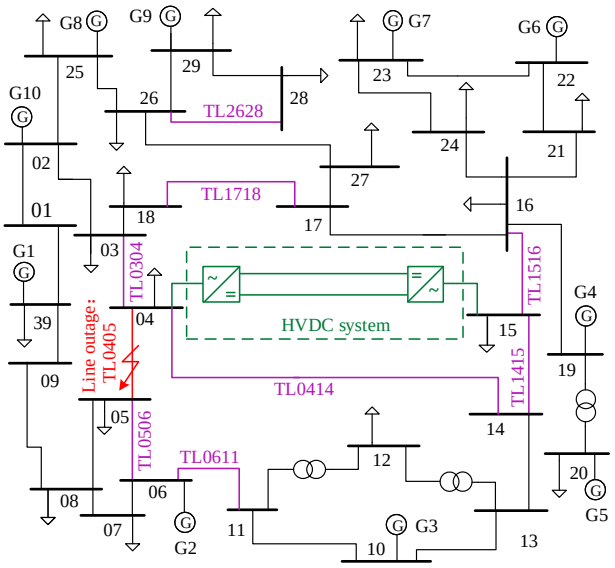

Fig. 3. Modified IEEE 39-bus system with HVDC links.

4.2 Calculation results of severity index for congestion management scenarios

Power congestion is easy to occur when N-1 fault occurs in power systems, so the N-1 scenario can also be understood as the possible congestion scenario. In this subsection, N-1 cases will be studied. During an N-1 situation, one AC line is out of service and then the power of the others is redistributed. IEEE 39-bus simulation model has 46 branches. The faults of 11 branches directly connected to the generator are not considered. Therefore, 35 N-1 cases are considered in this section.

Two control strategies based on the voltage angle droop controller will be used to compare with those without HVDC systems in 35 line outage scenarios. VAD controlled HVDC determines a fixed droop gain K for all N-1 cases by the OPF algorithm. This method obtains one constant global K for all N-1 cases. Optimal VAD controlled HVDC system determines individual K for each N-1 case.

A general optimal power flow (OPF) formulation for hybrid AC/DC systems was recently proposed in [13] and is employed in this paper to estimate the performance index for network congestion. The minimization of SI can be defined as the objective

function of OPF to alleviate the power congestion in the hybrid AC/DC system. It constructs a frame to adjust the droop gain K as the control variable to reduce the severity index in the network. Taking into account the limiting conditions, a set of constraints is added to OPF formulation.

The severity index result is visualized in Fig. 4. The severity index while without VAD control is the largest in most scenarios, except in scenario 22 and 23. Because the network structure changes in different N-1 situations, the VAD control with fixed *K* does not adapt to some scenarios. It also can be observed that the control effect of the optimal VAD control (red curve) is better than the VAD control (green curve). The red line at the bottom indicates that the severity index of this optimal VAD strategy is minimal. Fig. 5 illustrates the results of the droop gain *K*. The VAD controlled HVDC (green circle) sets a fixed droop gain *K* (-0.16) for all N-1 cases. For the optimal VAD control (red cross), it reveals the gain *K* has been adjusted for each different N-1 scenarios.

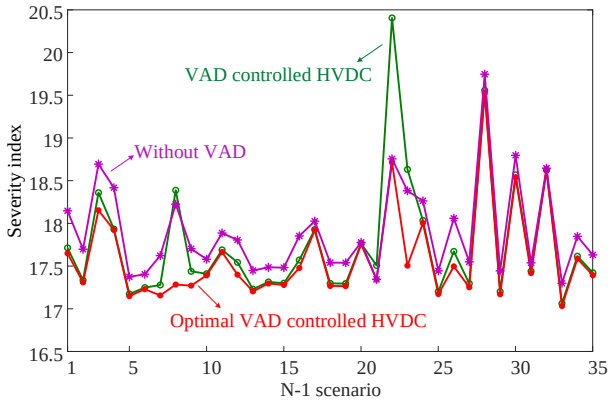

Fig. 4. The severity index results for the three control strategies.

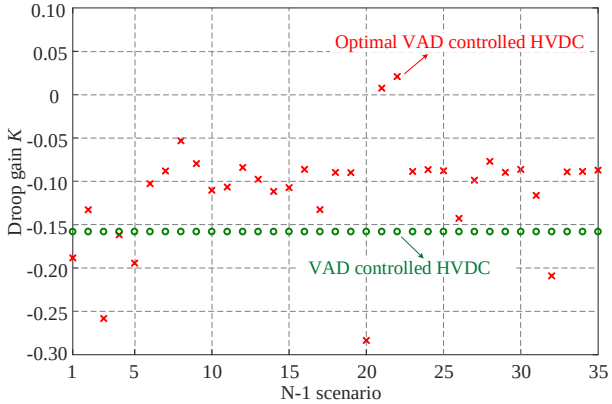

Fig. 5. The results of droop gain *K* under the VAD controlled HVDC and optimal VAD controlled HVDC.

When the topology of the system changes because of the line outage, the voltage angles in (2) also change. The optimal VAD controlled HVDC system adjusts the output power instruction of VSC station, which is conducive to a more reasonable distribution of power flow, thus reducing the overall severity index. Based on the aforementioned simulation results and evaluation analysis, it is obvious that optimal VAD control is more flexible and has more optimal performance index than VAD control. It verifies the effective curative congestion management of the proposed method to reduce the overload severity.

4.3 Dynamic characteristics analysis

In order to test the control performance and effect of the control method in the time domain, it is necessary to analyze the dynamic performance of the hybrid AC/DC system in the N-1 situation. This section reveals the dynamic behavior of the VAD-HVDC system and AC transmission lines in the modified New England test system.

4.3.1 Dynamic behavior in the VAD-HVDC system

In this subsection, we begins to focus on the specific dynamic process in the VAD-HVDC system after the line outage. When the AC transmission line TL0405 has a fault at 5 s (shown in Fig. 3), the dynamic responses in the VAD-HVDC system are presented in Fig. 6.

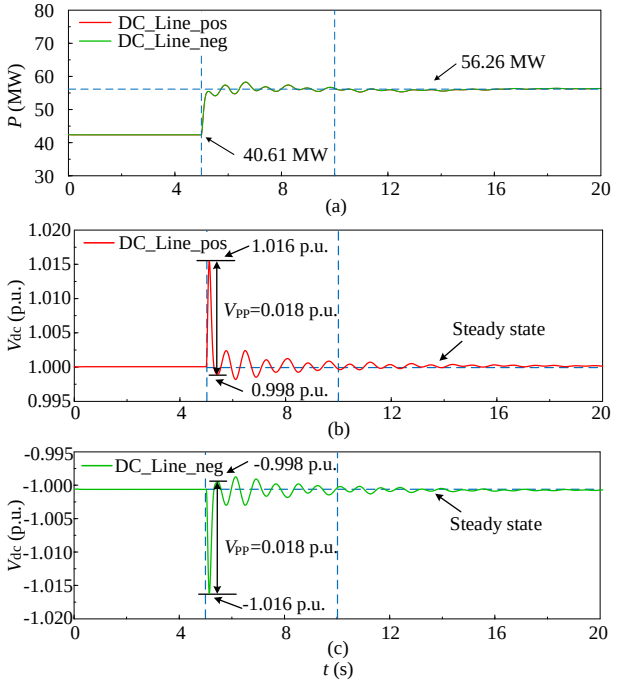

Fig. 6 When N-1 situation occurs on TL0405: (a) active power response on a single line of HVDC station; (b) voltage of the positive DC line in the HVDC station; (c) voltage of the negative DC line in the HVDC station.

The active powers on the DC cables in the HVDC station are illustrated in Fig. 6(a). The steady-state power before the fault is 40.61 MW. The N-1 scenario occurs at 5 s, and the VAD controller regulates the active power set-point by the control droop gain *K*. We set the control parameter *K* to -0.088. After the fault, the active power of a single DC cable is stabilized at 56.26 MW. In the VSC-HVDC system, the magnitude and orientation of transmitted power on positive and negative poles of the HVDC system are consistent. Therefore, the transmission power waveforms on the two poles overlap. It demonstrates that the total transmission power of the HVDC system adjusts from 81.22 MW to 112.52 MW.

When N-1 situation occurs, the power injected into VSC-station fluctuates due to the line fault. If the output power signal of the VSC station is not adjusted timely, the power balance is easy to be affected and the DC voltage will change drastically. Therefore, the DC voltage of the HVDC link is also an important indicator during the dynamic characteristics analysis.

Fig. 6(b) and (c) demonstrate in detail the DC voltages on the positive and negative lines. When the N-1 fault appears at 5 s, the DC voltage fluctuates. Then the voltage angle droop controlled HVDC system converges quickly and re-stabilized at 1.0 p.u.. As can be observed from Fig. 6(b), the maximum peak value is 1.016 p.u., and the maximum trough value is 0.998 p.u., and the peak-to-peak value V_{pp} which describes the range of voltage signal values is 0.018 p.u.. In addition, the DC voltage of the negative line is totally opposite to that of the positive line, as shown in Fig. 6(c). It indicates that the DC voltage can be stabilized efficiently by the VAD-HVDC system.

Therefore, the transient results in the HVDC system support that a good dynamic performance of fast recovery and against interference can be achieved by this control method of VAD-HVDC.

4.3.2 Dynamic responses on the AC transmission lines

After the above analysis of transient characteristics in the HVDC system, Fig. 7 reveals the dynamic response of the representative active powers on AC transmission lines when TL0405 is disconnected at 5 s.

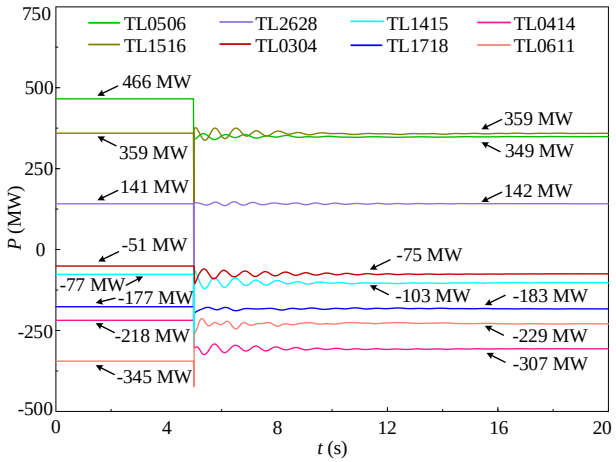

Fig. 7 The active powers on the AC transmission lines.

During the N-1 situation, three different types of active power transitions on the transmission lines are observed. The first type is the active power increase after the jump, e.g. TL0304, TL1415, TL1718, and TL0414. The second is the power reduction after the jump, e.g. TL1516 and TL2628. The third is that the power is almost unchanged after the jump, e.g. TL0506 and TL0611. It can be observed from the above that after the N-1 fault, the active powers on transmission lines under the control method can recover the steady state quickly. The active power results from Fig. 7 confirm that the hybrid power system can provide good stability under the control method.

To validate the control effect of the VAD controlled HVDC system for curative congestion management, Fig. 8 compares the dynamic response of the loading in critical lines after the N-1 fault occurs in the system without VAD-HVDC (green curve) and VAD-HVDC (red curve). In the system without VAD-HVDC, the TL0414 is overloaded, reaching 112.85%, and the TL1718 also has the highly loading of 91.29%. In the system with VAD-HVDC, the K value is adjusted as -0.088 at 5 s according to the calculation in Fig. 5. As a result, it can be observed from Fig. 8(a) that the overloaded line TL0414 is alleviated by means of the VAD-HVDC system (from 112.85% to 91.29%). In Fig. 8(b), the heavy loading of TL1718 is also reduced via the VAD-HVDC system (from 90.83% to 76.53%).

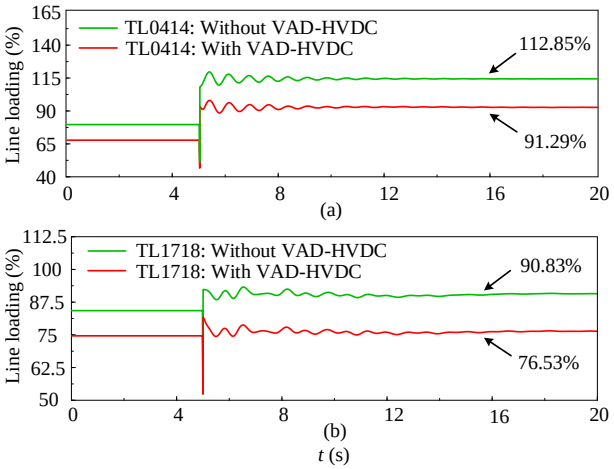

Fig. 8 Critical loadings when TL0405 is disconnected: (a) line loading of TL0414; (b) line loading of TL1718.

In this dynamic simulation, when the N-1 scenario occurs, the power flow distribution of the entire power grid is readjusted with ensuring no other new overloaded situations by regulating the gain K in the VAD controller, thereby effectively mitigating the critical loadings in the system.

5 Conclusion

This paper emphasizes the dynamic analysis of the hybrid AC/DC power system integrated with the VAD controlled HVDC system in curative congestion management scenarios. To start with a global control structure of the VSC-HVDC system based upon the VAD control is proposed. The severity index is assessed to verify the effective congestion management of the VAD control to reduce the overall severity index. Time-domain simulations are conducted via the modified IEEE 39-bus 10-machine system in DIgSILENT PowerFactory 2019. Based upon the dynamic characteristics analysis, a good dynamic performance of fast recovery and against interference can be achieved by means of the VAD control method and the DC voltage can be stabilized efficiently. Moreover, the AC active power responses confirm the hybrid power system providing good stability under the control method. The VAD controlled HVDC

system is able to alleviate effectively the critical loadings in the hybrid AC/DC system.

Considering communication time, some improvements to the advanced algorithm may be introduced to make timely actions and adjustments for unforeseen events in a fast and real-time manner.

This work was supported in part by China Scholarship Council (CSC) under Grant CSC No. 201706130143. The authors would like to thank Chong Di from Lappeenranta University of Technology and Jieying Zhang from Hunan University for their contributions to this work.

References

1. ENTSO-E, *Ten-Year Network Development Plan (TYNDP) 2018* (2018)
2. A. Kumar, K. R. Mittapalli, Int. J. Electr. Power **57**, 49 (2014)
3. A. Mishra, V. N. Kumar, J. Electr. Syst. Inform. Tech. **4**, 198 (2017)
4. L. L. Lai, *Power system restructuring and deregulation: trading, performance and information technology* (John Wiley & Sons, London, 2001)
5. A. K. Marten, D. Westermann, *2013 IEEE Power & Energy Society General Meeting* (2013)
6. A. K. Marten, D. Westermann, M. Luginbuhl, H. F. Sauvain, *2013 IEEE Grenoble Conference* (2013)
7. K. Frey, P. Wiest, K. Rudion, J. Christian, *2016 IEEE Power and Energy Society General Meeting* (2016)
8. K. Frey, K. Rudion, J. Christian, *IEEE International Energy Conference* (2016)
9. S. S. H. Yazdi, M. Jafar, H. Seyed, R. Kumars, Int. J. Electr. Power **102**, 272 (2018)
10. F. Sass, T. Sennewald, F. Linke, D. Westermann, Global. Energ. Interconnect. **1**, 585 (2018)
11. N. Amjady, M. Hakimi, Energ. Convers. Manage., **58**, 66 (2012)
12. M. Benasla, T. Allaoui, M. Brahami, V. K.Soode, M. Denaï, Electr. Pow. Syst. Res. **168**, 228 (2019)
13. F. Sass, T. Sennewald, D. Westermann, IEEE Trans. Power Syst. (2019)
14. Y. Zhou, S. Dalhues, J. Liu, C. Rehtanz, *IECON 2019 - 45nd Annual Conference of the IEEE Industrial Electronics Society* (to be published)
15. W. Wang, M. Bares, IEEE Trans. Power Syst., **29**, 1721 (2014)
16. P. L. Francos, S. S. Verdugo, H. F. Alvarez, S. Guyomarch, J. Loncle, *2012 IEEE Power and Energy Society General Meeting* (2012)
17. A. J. Wood, B. F. Wollenberg, *Power Generation, operation, and control*, John Wiley & Sons (New York, 1996)
18. S. C. Müller, U. Häger, C. Rehtanz, IEEE Trans. Ind. Inform. **10**, 2290 (2014)
19. R. N. Banu, D. Devaraj, Int. J. Electr. Electron. Eng. **3**, 552 (2009)
20. DIgSILENT GmbH, *DIgSILENT PowerFactory 2019 User Manual* (2018)
21. DIgSILENT GmbH, *DIgSILENT PowerFactory 2018 Techinical Reference Documentation Phase Measurement Device ElmPhi_pll* (2017)